Chemical Engineering Journal 529 (2026) 173109

Contents lists available at ScienceDirect

Chemical Engineering Journal

journal homepage: www.elsevier.com/locate/cej

# Revealing the sodium storage capacity, kinetics, and sodium plating signals of hard carbon

Wei Li [a], Shini Lin [a], Yuejing Zeng [a], Yuan Qin [a], Honghao Xie [a], Xing Chen [a], Jing Zeng [a,*], Peng Zhang [b,*], Jinbao Zhao [a,*]

[a] State-Province Joint Engineering Laboratory of Power Source Technology for New Energy Vehicle, State Key Laboratory of Physical Chemistry of Solid Surfaces, Engineering Research Center of Electrochemical Technology, Collaborative Innovation Center of Chemistry for Energy Materials, College of Chemistry and Chemical Engineering, Ministry of Education, Xiamen University, Xiamen, 361005, China
[b] College of Energy & School of Energy Research, Xiamen University, Xiamen, 361102, China

ARTICLE INFO

*Keywords:*
Sodium-ion batteries
Hard carbon
Capacity calibration
Early warning signal
Battery design

ABSTRACT

Sodium-ion batteries (SIBs) have become the most promising technology in large-scale energy storage applications. Among various anodes, hard carbon (HC) has an absolute advantage because of its high capacity and low potential. However, the lifespan and safety of SIBs are severely compromised by sodium plating and other detrimental effects, primarily caused by inaccurate capacity determination leading to N/P ratio mismatch. This study systematically investigated the detrimental impacts of sodium metal polarization on capacity assessment. Building upon these findings, we developed an over-sodiation protocol to precisely quantify the capacity of HC anodes by monitoring the "transition point" where electrochemical behavior shifts from sodium storage to sodium plating. Furthermore, this method has been rigorously validated across multiple HC material systems, and the relationship between different HC capacities and rate performance was evaluated. Subsequently, through comprehensive statistical analysis of structural parameters and kinetic characteristics, we obtained crucial insights for optimizing HC structures to enhance sodium-ion transport kinetics. Finally, based on this transition of electrochemical behavior, an early warning signal for sodium plating was proposed to indicate capacity fading and safety variations in SIBs. The insights proposed in this study could provide valuable design principles for HC materials development and SIBs performance enhancement.

## 1. Introduction

Lithium-ion batteries (LIBs) have achieved great success owing to their widespread use in portable energy storage and electric vehicles [1–5]. Over the past decades, the global shift toward renewable energy has established large-scale energy storage as a key technological enabler, driving intensive research efforts to address the growing mismatch between energy generation and demand [6–8]. However, the challenges such as limited lithium resource and inadequate low-temperature performance in commercial LIBs have created an urgent demand for developing new energy storage paradigms [9,10]. To address these limitations, sodium-ion batteries (SIBs) have emerged as a promising solution, capitalizing on their naturally abundant raw materials and extended operational temperature range (−40 °C to 80 °C) for sustainable energy storage systems [11–14].

The advancement of SIBs critically depends on three fundamental aspects: (i) cathode/anode materials with high specific capacity and favorable kinetics, (ii) rational cell architecture design, and (iii) optimized electrode-electrolyte interfaces, which collectively determine their practical viability for grid-scale energy storage [15,16]. Current cathode research primarily focuses on layered transition metal oxides [17,18], polyanion compounds [19,20], Prussian blue analogues [21]. While each system exhibits distinct advantages in terms of energy density, structural stability, or cost-effectiveness, none has yet demonstrated clear superiority for commercial deployment [22]. For anode materials, hard carbon (HC) demonstrates superior performance owing to its low sodiation potential and high reversible capacity [23–25]. Notably, Hu et al. synthesized HC using phenol-formaldehyde resin as the precursor and ethanol as the pore-forming agent, and the phenolic resin-derived HC exhibited a high Na storage capacity of approximately 410 mAh $g^{-1}$ [26]. In addition, the HC optimized by Zhang et al. through the transient sintering strategy exhibits an extremely high platform

* Corresponding authors.
*E-mail addresses:* zengjing@xmu.edu.cn (J. Zeng), pengzhang@xmu.edu.cn (P. Zhang), jbzhao@xmu.edu.cn (J. Zhao).

https://doi.org/10.1016/j.cej.2026.173109
Received 29 October 2025; Received in revised form 23 December 2025; Accepted 15 January 2026
Available online 18 January 2026

capacity of 325 mAh $g^{-1}$, which increases the energy density of SIBs by 20.7% [27]. Zhao et al. leveraged ultra-affordable asphalt as a precursor, combined with pre-oxidation treatment to specifically tailor the microstructures of HC, achieving an impressive carbon yield of 63% [28].

However, there has been no unified standard for capacity calibration of HC materials so far. As shown in Table S1, different charging and discharging conditions have been employed across different research endeavors. Significant discrepancies are observed in the reported capacities of HC when different evaluation protocols are employed (Fig. S1). Alarmingly, in the Na||HC half-cell systems using ester electrolytes, the excessive polarization potential of sodium metal frequently results in an underestimation of the capacity of HC materials, particularly at higher current densities [29–34]. Inaccurate capacity calibration can lead to an imbalanced N/P ratio during battery design, which may decrease energy density or cause sodium plating. Sodium plating not only leads to the rapid capacity degradation of the battery but also causes the generation of reducing gas inside the battery, seriously deteriorating the safety of the battery (Fig. S2 and S3). Therefore, accurate capacity calibration or precisely determining the boundary between effectively utilizable sodium storage capacity and undesirable sodium plating behavior is crucial for the rational design and application of SIBs [35]. Moreover, this boundary could be also correlated with structural parameters of HC materials to guide the design of superior anode with higher utilizable capacity and faster kinetics.

Herein, three commercial HC materials with pseudo-graphitic microdomains and micropores are used as research models (marked as K-HC, Y-HC and N-HC, respectively). Through systematic characterization, the three HC variants demonstrate distinct yet subtle variations in closed-pore volume and interlayer spacing, making them ideal models to investigate structure-dependent sodium storage mechanisms and their critical thresholds. In-situ XRD and Raman spectroscopy were used to monitor the structural evolution of their sodiation process and further investigate the sodium storage mechanism. Experimental results have shown that all of HC materials follow the “adsorption-intercalation-filling” mechanism for sodium storage. Through comprehensive electrochemical evaluations employing three-electrode cells, Na metal symmetric cells, HC symmetric cells, and full-cell configurations, we have conclusively identified that the substantial polarization of sodium metal in ester-based electrolyte serves as the predominant factor responsible for the compromised capacity performance of HC, consequently resulting in imprecise capacity determination. Herein, we developed a capacity-cutoff testing protocol that precisely controls the sodiation state. Under controlled over-sodiation conditions, we decoupled the characteristic electrochemical signatures in the plateau region, distinguishing between reversible sodium storage and metallic sodium plating behaviors. Importantly, we identified the critical plateau inflection point between these two distinct processes. Based on these findings, we proposed the utilizable capacity boundary for effective sodium storage, or in other words, the metallic sodium plating threshold of HC anode. Subsequently, the accuracy and universality of such utilizable capacity boundary were further verified through in-situ XRD, post-mortem analysis, and capacity cut-off cycling. The remarkable cycling stability exhibited by cells operating within this capacity boundary provides definitive evidence for its efficacy as a precise capacity calibration standard for HC anodes. Furthermore, the structural design principles based on the boundary were discussed to guide the material design, thus expanding the available kinetic boundary of HC in the actual electrochemical process. Finally, based on this change in electrochemical behavior, a warning signal for sodium plating behavior was proposed. This work provides constructive insights into the development and application of long-life and high-safety SIBs from multiple perspectives, including HC structure regulation, battery design, and sodium plating warning.

## 2. Results and discussion

### 2.1. Structural characterization and sodium storage mechanism of HC

In this study, three commercial HC materials (K-HC, Y-HC, and N-HC) were used as case models to systematically investigate the sodium storage mechanism, the sodium plating threshold, and sodium storage kinetics. In order to correlate the electrochemical information of HC materials with their microstructure, various material characterization methods were used to analyze the microstructure of HC materials. As shown in Fig. S4, three types of HC materials exhibited similar block-like morphology observed by scanning electron microscopy (SEM). High resolution transmission electron microscopy (HRTEM) was used to observe the microstructure of HC materials, and all three types of HC were composed of locally twisted pseudo-graphite microdomains and closed nanopores, exhibiting structural characteristics of short-range order and long-range disorder (Fig. 1(a-c)). The XRD patterns exhibit two broad diffraction peaks corresponding to the (002) and (100) peaks. In addition, Y-HC exhibits a peak similar to graphite around 26.5°, indicating the presence of graphite structure (Fig. 1(d)). This graphite structure will prevent the insertion of $Na^+$, so the presence of graphite structure does not affect the analysis of the sodium storage mechanism [36]. By combining XRD patterns with TEM images, the basic structural parameters of HC materials can be calculated, including average layer spacing ($d_{002}$), average layer stacking distance ($L_c$), the longitudinal size of structure ($L_a$), and the number of layers stacked in parallel ($N$) (Fig. S5, Table S2). Raman spectroscopy was employed to assess the structural ordering of HC, where a higher intensity ratio of the D-band to G-band ($I_D/I_G$) corresponds to increased structural disorder (Fig. S6, Table S2). To characterize the pore structure of HC, we performed comprehensive analysis using small angle X-ray scattering (SAXS) measurements, true density tests, and $N_2/CO_2$ adsorption-desorption experiments, thereby obtaining quantitative data on closed-pore volume, average open-pore diameter, and specific surface area (Fig. 1(e, f) and S7, Table S3). The results from $N_2$ and $CO_2$ adsorption-desorption tests reveal that all three types of HC materials possess a predominantly mesoporous structure, with negligible contents of micropores and ultra-micropores. Pore size distribution analysis based on the Barrett-Joyner-Halenda (BJH) method applied to the desorption branch of the nitrogen isotherms indicates that K-HC possesses the largest average pore diameter, whereas Y-HC possesses the smallest. This difference in pore size is expected to influence $Na^+$ diffusion pathways within the material and consequently affect the sodium storage kinetics. Furthermore, analysis combining SAXS and true density measurements shows that N-HC exhibits the largest closed-pore volume, while Y-HC exhibits the smallest. This parameter is closely related to the plateau capacity observed in the electrochemical performance. Based on these pore structure characteristics, we selected K-HC—which demonstrates excellent performance—as the primary focus for subsequent investigation, with the other two materials serving as auxiliary references.

In situ XRD and Raman spectroscopy were employed to systematically investigate the detailed sodiation mechanisms in various HC materials. In the in-situ XRD test, the (002) peak of HC in the XRD patterns showed no significant shift throughout the entire sodiation and desodiation process, which may indicate that the pseudo-graphite layer is large enough to store $Na^+$ (Fig. 1(g)). Meanwhile, the intensity of the (002) peak of HC gradually decreased during the sodiation process, which is caused by the insertion of $Na^+$ between the pseudo-graphite layers [37,38]. What's more, in-situ Raman spectroscopy provides more information on $Na^+$ storage procedure (Fig. 1(h, i)). During the sodiation process, the G band shows a progressive red-shift (negative shift). Compared with graphite materials in LIBs, the weakening of the C—C bond due to the insertion of $Li^+$ into the graphite carbon layer could lead to a red shift in the G band [39]. Therefore, it can also assist in explaining the occurrence of sodium insertion behavior in the sodium storage process of HC materials. In addition, the adsorption of $Na^+$ on

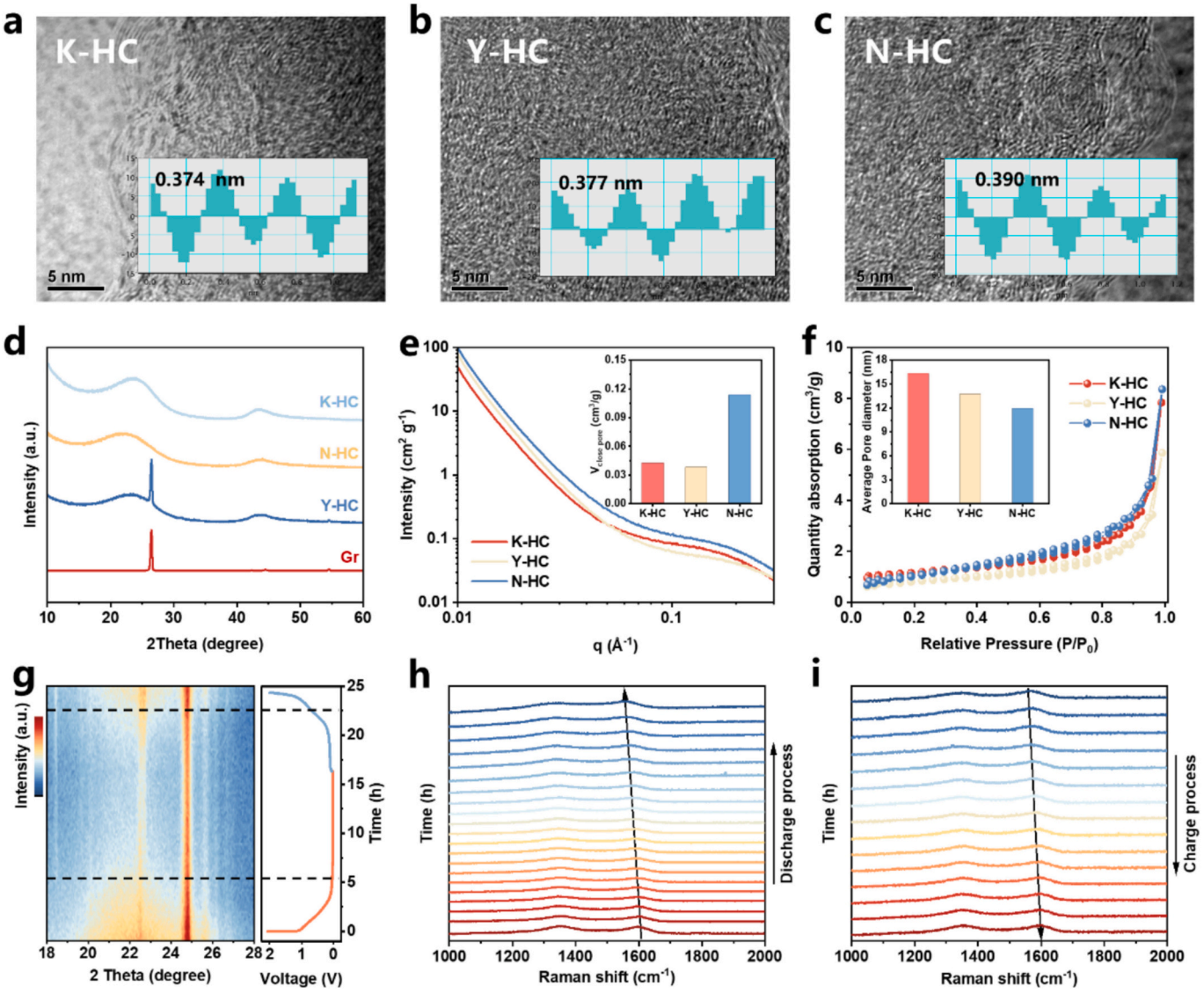


**Fig. 1.** Structural characterization of HC: HRTEM image of (a) K-HC, (b) Y-HC, (c) N-HC (the insets show the intensity line profile images). (d) XRD pattern. (e) SAXS profiles (the insets show the closed-pore volume derived from density measurements). (f) $N_2$ adsorption-desorption isotherms (Average open-pore diameter derived from the BJH desorption branch). (g) In situ XRD patterns during the first discharge-charge process of HC. (h, i) In situ Raman mappings in the initial discharge-charge process of HC.

defect sites and the filling of closed nanopores will further reduce the number of defect sites in HC, and also cause a red shift in the G band [27]. Consequently, during desodiation, persistent $Na^+$ adsorption at defect sites and residual sodium cluster occupation within nanopores are observed. The electrochemical formation of sodium clusters within the nanopores was directly verified by potential-dependent colorimetric analysis (Fig. S8). Subsequently, X-ray Photoelectron Spectroscopy (XPS) measurements were performed to investigate the bonding states of intercalated sodium in HC. As shown in Fig. S9, a characteristic peak appears at approximately 1071 eV in the Na 1s spectrum, which corresponds to the Na – O – C species and confirms the existence of $Na^+$ adsorption on surface defects. With the increase of etching depth, the position of the Na 1 s peak shifts toward higher binding energy, indicating that the sodium species in HC possess a higher binding energy that is closer to that of metallic sodium. This phenomenon verifies the coexistence of $Na^+$ and quasi-metallic sodium in the electrode [36,40]. In summary, the detailed sodium storage mechanism of "adsorption-intercalation-filling" in various HC has been confirmed. During the sodium storage process, sodium ions are first intercalated between the layers and then adsorbed on the defect sites and open pores (slope region), and then fill the pores (plateau region), which establishes a fundamental basis for further mechanistic investigation.

### 2.2. Plateau inflection point and performance evaluation of HC

In addition to the ambiguous mechanism of sodium storage in HC, the boundary between the effectively utilizable sodium storage capacity and undesirable sodium plating behavior as well as the relationship between such boundary and kinetics of $Na^+$ in HC materials are also consistently misunderstood. Evaluating the capacity performance of Na||HC half-cells at different current densities is a traditional method for assessing the sodium storage kinetics of HC. However, in ester electrolytes, the capacity performance of Na||HC half-cells is surprisingly poor (Fig. 2(a) and S10), which has been observed in other literature as well [41–43]. When ether electrolytes are used instead, the capacity performance of HC is significantly improved (Fig. S11(a-d)). This phenomenon has also been extensively reported, but it is more often explained by the high impedance of the SEI on the HC in ester electrolytes [31,44–46]. Herein, we fabricated a 5 Ah-class pouch-type full cell employing $Na_3Fe_2(PO_4)(P_2O_7)$ (NFPP) cathode and K-HC anode in ester-based

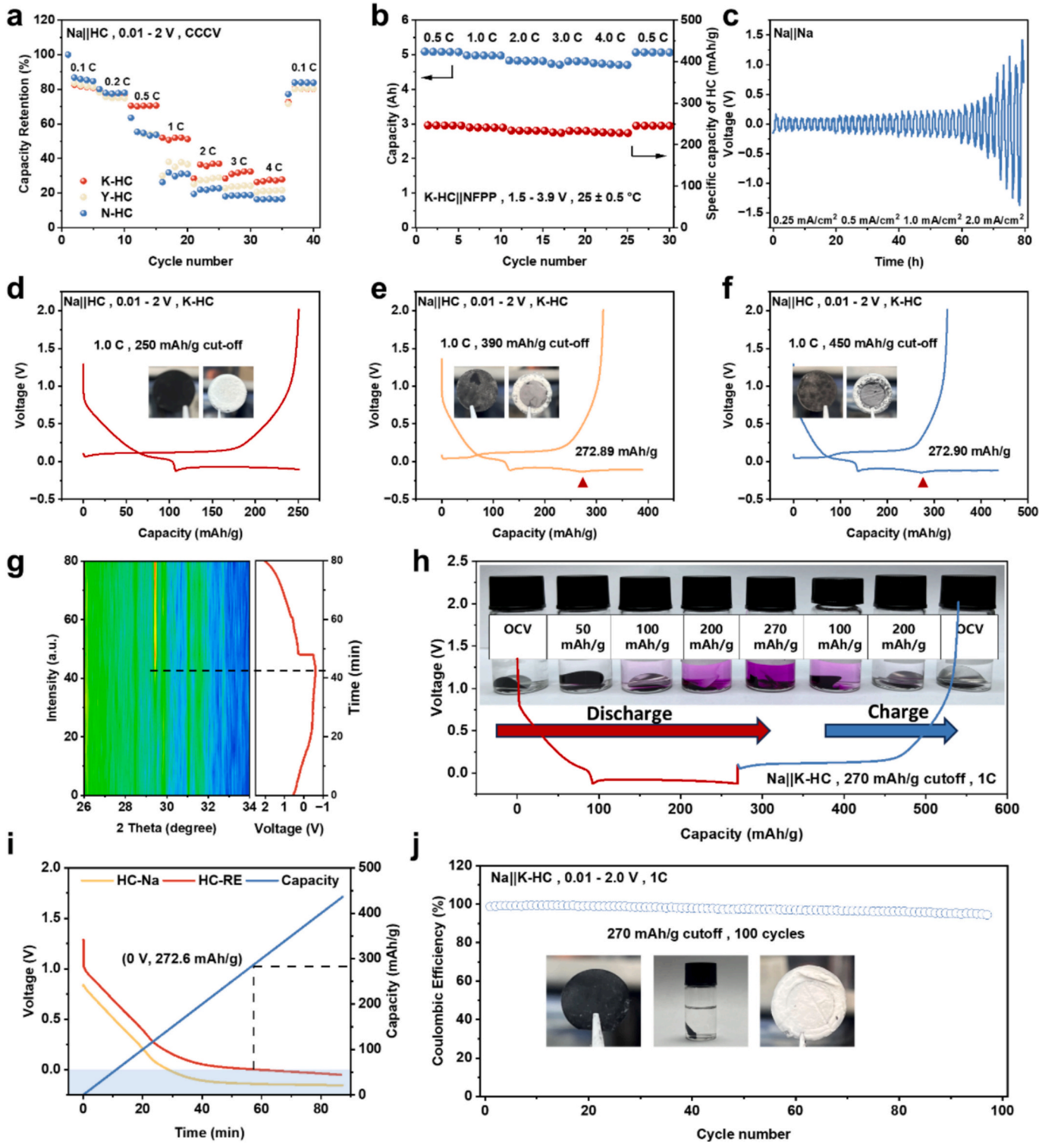


**Fig. 2.** (a) Rate performance of Na||HC half-cells. (b) Rate performance of HC||NFPP pouch cell. (c) Cycling performance of Na||Na symmetrical cells with the ester electrolyte using different current density. (d-e) Voltage-capacity curves at different discharge cut-off capacity (inset shows the HC and separator of the Na||HC half cells after 10 cycles). (g) In-situ XRD patterns of HC during the over-sodiation and de-sodiation process at 1.0C. (h) Colorimetry experiment of HC at different potentials with different cutoff capacities. (i) Voltage-time curves of three-electrode Na||HC half-cell during sodiation process. (j) Coulombic efficiency of Na||HC half-cell with discharge cut-off capacity of 270 mAh g-1 at the rate of 1.0C (inset shows the HC electrode, colorimetry experiment of HC electrode, and separator after 100 cycles).

electrolyte (Fig. S12, more detailed cell information is shown in Table S4). This K-HC||NFPP full cell exhibits excellent capacity stability when charged and discharged at a rate of 0.5–4.0C, and at a charge/discharge rate of 4.0C, the capacity can still reach approximately 4.7 Ah (Fig. 2(b)). Converting the capacity of the full cell to the capacity of HC, the rate characteristics of the K-HC||NFPP full cell are far superior to those of the Na||HC half-cell (The HC materials achieve the capacity of 245.5 mAh $g^{-1}$ and 230.6 mAh $g^{-1}$ at 0.5C and 4.0C in full cell,

respectively). Therefore, sodium metal reference electrode may be the key factor causing this phenomenon. The charge and discharge cycles of Na||Na symmetrical cells assembled with ester and ether electrolytes demonstrate that the polarization potential of sodium metal in ester electrolytes is much higher than that in ether electrolytes (Fig. 2(c) and S11(e)). Additionally, in the Tafel curves of symmetric Na||Na symmetrical cells, sodium metal exhibits a higher exchange current density in ether-based electrolytes, indicating faster interface deposition kinetics (Fig. S11(f)). Finally, we disassembled the Na||HC half-cells with different electrolytes (ester and ether) after 5 cycles and reassembled HC||HC symmetrical cells with the corresponding electrolytes. Through EIS testing, it can be found that HC has similar charge transfer resistance ($R_{ct}$) in different electrolytes (Fig. S13). This also indicates that the interfacial impedance of HC in different electrolytes of the Na||HC half-cells is not the reason for the huge differences in its electrochemical performance. In conclusion, there are significant misunderstandings in using conventional Na||HC half-cells to evaluate the capacity of HC, the characteristics of SEI on HC, as well as the properties of the electrolyte.

Consequently, a reliable and practical methodology is required to accurately assess the intrinsic capacity of HC in ester-based electrolytes. We posit that the transition between sodium storage and metallic plating in HC exhibits distinct electrochemical signatures, which could serve as definitive indicators for delineating these two processes. We investigated the sodium storage boundary of HC by employing a controlled constant-current discharge protocol coupled with capacity cutoff (Na||HC half-cells are used for testing, and the charge-discharge rate is 1.0C). When the cut-off capacity is 250 mAh $g^{-1}$, the voltage reaches 0 V when the sodium storage capacity (plateau region) is only 107 mAh $g^{-1}$, but after 10 cycles, the cell does not experience sodium plating (Fig. 2(d)). This indicates that for Na||HC half-cells, a voltage below 0 V does not indicate the occurrence of sodium plating. When the cut-off capacity increases to 390 mAh $g^{-1}$ and 450 mAh $g^{-1}$, it is obvious that there are two inconsistent plateaus with a clear "inflection point" in the plateau region of the sodiation curve (Fig. 2(e, f)). It could be identified that the capacity at the "inflection point" is approximately 272.9 mAh $g^{-1}$. This "inflection point" is the lowest point of the voltage on the sodiation curve (capacity-voltage curve) of the Na||HC half-cell. The occurrence of sodium plating was confirmed through post-mortem analysis. Therefore, we speculate that these distinctive platforms represent two electrochemical behaviors, sodium ions storage and sodium metal plating, respectively. Further, the HC of Na||HC half-cells at different stages of sodiation were observed by SEM, and it was indeed found that the HC capacity of 272.9 mAh $g^{-1}$ was the boundary between the absence and presence of sodium plating (Fig. S14). Solid-state nuclear magnetic resonance spectroscopy (ssNMR) further confirmed that the surface deposits were metallic sodium plating (Fig. S15). In addition, in-situ XRD was used to monitor the time of sodium plating on the surface of HC during the sodiation processes (Fig. 2(g)). When Na||HC half-cell is discharged for 40 min, an inflection point can be clearly observed, and at the same time, the diffraction peak of sodium metal appears at 29° in the in-situ XRD pattern [47]. Finally, we further demonstrated this sodium storage boundary through colorimetric experiments combined with comparative experiments (Fig. 2(h) and S16). When Na||HC half-cells are discharged with the terminated capacities of 270 mAh $g^{-1}$ and 400 mAh $g^{-1}$ respectively and charged to 2.0 V, HC exhibits completely different phenomena in the colorimetric reagent. When the cut-off capacity is 270 mAh $g^{-1}$, the colorimetric reagent turns red first and then colorless during the sodiation and de-sodiation process. When the cut-off capacity increases to 400 mAh $g^{-1}$, the colorimetric reagent turns red first and then keeps light red during the sodiation and de-sodiation process, and it does not turn back to colorless when completing desodiation. This also indicates the occurrence of irreversible sodium plating behavior. The above post-mortem analysis, in-situ XRD testing, and colorimetric experiments all confirm that the "inflection point" near 272.9 mAh $g^{-1}$ is the boundary between sodium storage and metallic sodium plating, and the two platforms before and after the "inflection point" also represent the two different electrochemical behaviors with distinct electrochemical reversibility characteristics. Therefore, the capacity at the plateau inflection point can be regarded as the precise sodium storage capacity of HC.

In order to separate the influence of sodium metal polarization on the charging and discharging process of the Na||HC half-cells, and once again demonstrate the accuracy of "inflection point" for HC capacity evaluation, a Na reference electrode (RE) was added to the Na||HC half-cell. As shown in Fig. 2(i), when the voltage of HC (vs. RE) is 0 V, the capacity of HC is 272.6 mAh $g^{-1}$ at a discharge rate of 1.0C, the result is consistent with the conclusions of previous tests and analyses. Subsequently, the Na||HC half-cell underwent 100 cycles with a cut-off capacity of 270 mAh $g^{-1}$ (Fig. S17). At the beginning of the cycle, the coulombic efficiency remains above 99%, and throughout the entire cycle, the coulombic efficiency is greater than 95% (Fig. 2(j)). The reason for the decrease of coulombic efficiency in the later stage of the cycle is that the polarization of sodium metal increases as the cycle progresses (Fig. S18). After 100 cycles, post-mortem analysis of the Na||HC half-cell showed that there was no metallic sodium plating on the surface of the HC and separator, and the colorimetric reagent containing the HC did not show any discoloration (Fig. 2(j) and S19). In summary, the over-sodiation strategy with capacity control can achieve precise calibration of HC capacity through the transition (inflection point) between sodium storage and sodium plating behaviors.

To demonstrate the universality of the "inflection point" as the sodium storage boundary, Y-HC and N-HC were also used in different discharge capacity cutoff experiments (Fig. 3(a-f)). In the over-sodiation experiment with a high cutoff capacity, obvious "inflection points" were observed in both Y-HC and N-HC, and the capacities at the inflection points of the same material were relatively consistent. This plateau inflection point can serve as a demarcation boundary between the effectively utilizable sodium storage capacity and undesirable sodium plating behavior. On this basis, the three types of HC exhibit different "inflection point" position at a rate of 1.0C. The capacities corresponding to the "inflection point" of K-HC, Y-HC, and N-HC are approximately 272.9 mAh $g^{-1}$, 242.2 mAh $g^{-1}$, and 278.1 mAh $g^{-1}$, respectively. Post-mortem characterization was performed after 10 cycles of the Na||HC half-cells, and the charge-discharge curves were shown in Fig. S20. Notably, the inflection-point-derived capacities exhibit exceptional cycling consistency over the 10 cycles, indicating highly stable and reversible sodium storage behavior. Therefore, through the over-sodiation (or over-discharge) strategy in Na||HC half-cells, the effectively utilizable sodium storage capacity boundary of HC materials has been successfully and accurately identified, which enables the rational utilization of HC materials and prevents sodium plating at the thermodynamic level.

The over-sodiation strategy can also be used to test the kinetic characteristics of HC. We systematically studied the capacity performance of different HC materials at different rates by adopting the over-sodiation strategy, further expanding the universality of this strategy (Fig. 3(g-i), S21 and S22). Through statistical analysis and fitting of the rate characteristics of the three types of HC, their rate responsiveness was obtained (i.e., the slope of the fitted line. The Pearson's correlation coefficients (r) of the fitted lines for the three types of HC are all close to −1, indicating a strong linear relationship between the two variables [48]). The slope of the linear trend can serve as an indicator of kinetic performance, where a smaller slope signifies better rate capability with less capacity loss at increasing current densities. After comparison, it can be clearly identified K-HC exhibits the best rate performance, while N-HC has the worst rate performance (Fig. 3(j)). In addition, the over-sodiation methodology offers superior applicability for capacity standardization of HC electrodes under varying electrolyte formulations, electrode configurations, and operating parameters (Fig. 3(k)). For example, through this strategy, the difference in capacity performance of HC in ether-based and ester-based electrolyte systems was determined (Fig. S23).

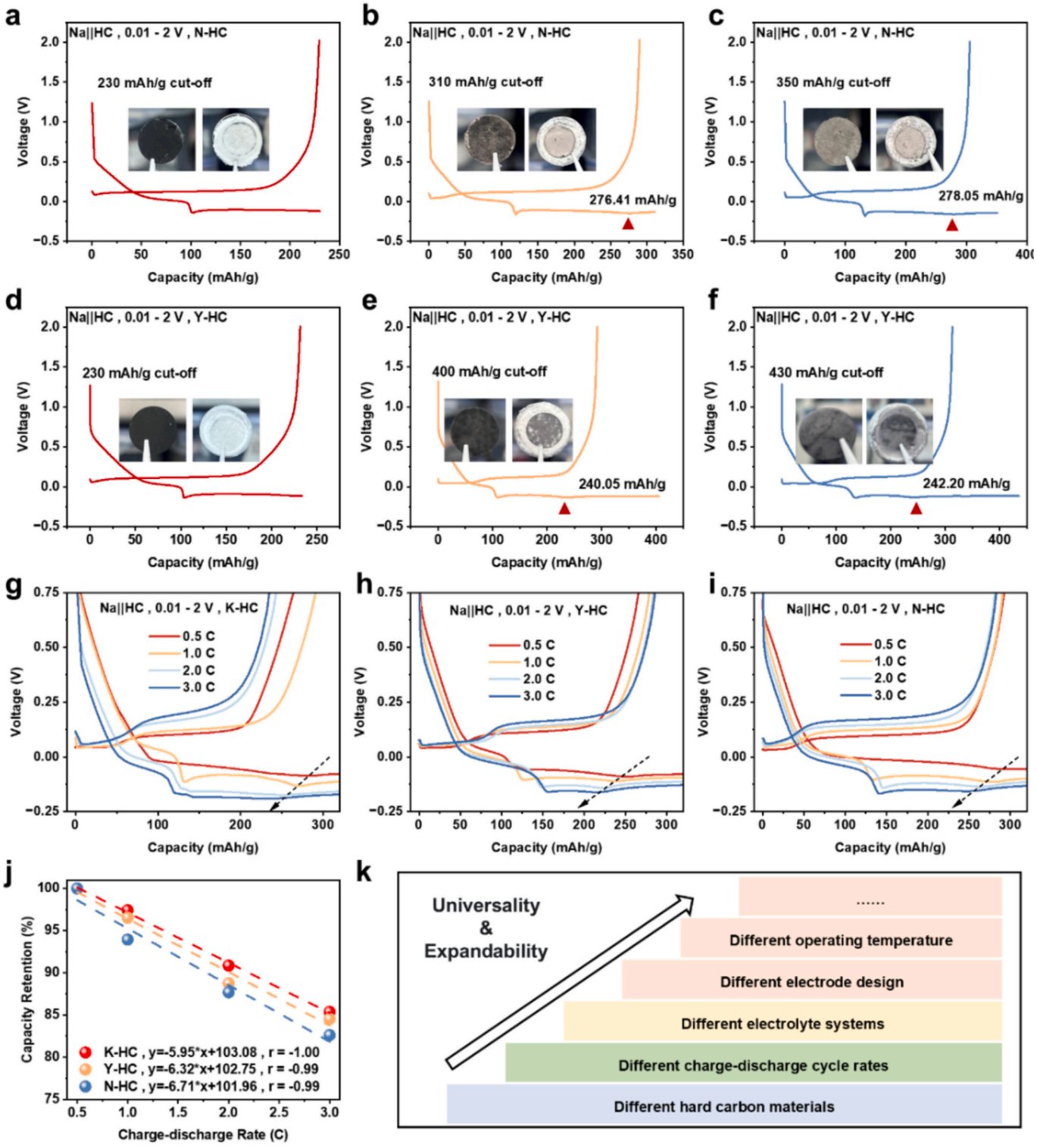


**Fig. 3.** Voltage-capacity curves of (a-c) Y-HC and (d-f) N-HC at different discharge cut-off capacity (inset shows the HC and separator of the Na||HC half cells after 10 cycles). (g-h) The capacity performance of Na||HC half-cells at different cycling rates is calculated based on the over-sodiation strategy. (j) The rate responsiveness of three types of HC. (k) Schematic diagram of the universality and expandability of the "inflection point" as the boundary of reversible sodium storage capacity.

### *2.3. Performance-structure relationship of HC*

As established, we have clearly demonstrated that different HC materials exhibit distinct rate capability performance, which is highly likely correlated with their structural characteristics. In this study, the electrochemical performance (especially the kinetic characteristics of sodiation) of three commercial HC materials was correlated with their structural characteristics. The galvanostatic intermittent titration technique (GITT) was used to test the sodium storage kinetics of HC materials (Fig. S24). As shown in Fig. 4(a), the $Na^+$ diffusion coefficients of the three types of HC materials exhibit a consistent trend, and there is no significant difference in order of magnitude. During the sodiation process, the diffusion coefficient of $Na^+$ slowly changes in the slope region. When the voltage drops to 0.1 V, the diffusion coefficient sharply

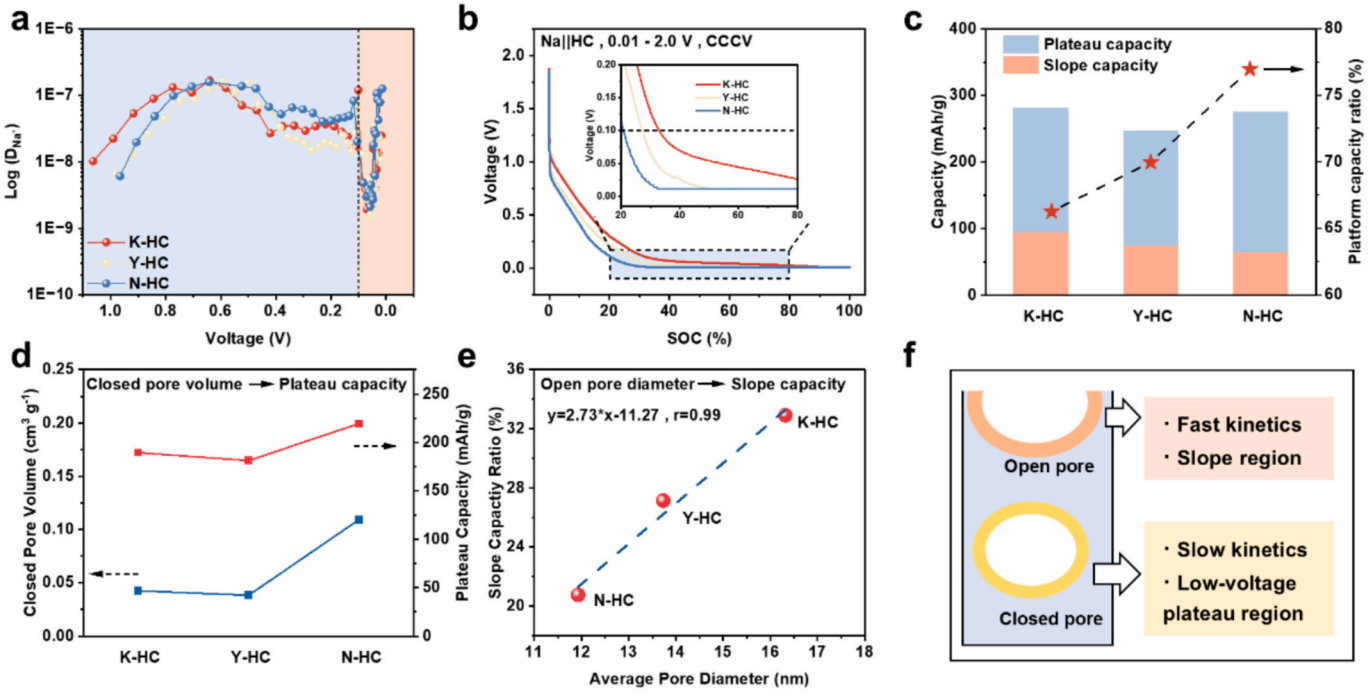


**Fig. 4.** (a) The Na + diffusion coefficient calculated from GITT during the sodiation process. (b) Voltage-SOC curves of sodiation process. (c) The capacity contributed from slope and plateau region calculated from voltage-capacity curve. (d) Closed pore volume and platform capacity of three types of HC. (e) The relationship between the average pore diameter and slope capacity ratio of three types of HC. (f) A schematic diagram of the relationship between the open pores and closed pores of HC and the sodium storage kinetics is provided to guide more rational material design.

decreases to its minimum value and then significantly increases. Therefore, HC materials have relatively poor sodium storage kinetics in the plateau region, while the kinetics are faster in the slope region. Simultaneously, the plateau voltage approaches 0 V. When the sodiation current increases, sodium plating is highly probable.

In order to clarify the correlation between the structural characteristics and capacity characteristics of HC, we verified it through a method of comparative statistics. Through low-current charging and discharging, the capacity of HC was divided into the slope capacity and the plateau capacity, with 0.1 V as the demarcation (Fig. S25). The plateau capacity of K-HC, Y-HC, and N-HC is 189.35 mAh $g^{-1}$, 181.19 mAh $g^{-1}$, and 219.32 mAh $g^{-1}$, respectively (Fig. 4(b, c)). After statistical comparison, the plateau capacity of HC is positively correlated with the closed pore volume (Fig. 4(d)), and a larger closed pore volume will lead to a larger plateau capacity, which is consistent with the conclusions of the sodium storage mechanism proposed in the previous text. In conclusion, the increase in closed pore volume during the HC design process helps to enhance the plateau capacity, thereby improving the energy density of the battery under defined conditions. However, it also reduces the rate performance of the battery.

Besides, HC materials with a larger proportion of slope capacity often exhibit excellent rate characteristics. Through statistical comparison, the proportion of slope capacity of the three types of HC is positively correlated with the average open pore diameter, that is, appropriately increasing the pore diameter of HC can help improve sodium storage kinetics (Fig. 4(e)). This is because larger pore sizes of HC help promote the pseudo-capacitive adsorption of $Na^+$ and the wettability of the electrolyte [49,50]. Meanwhile, the larger open pore volume will induce a higher sodium storage voltage and reduce the risk of sodium plating. In summary, the increase in closed pore volume during the HC design process helps to enhance the plateau capacity, thereby improving the energy density of the battery. However, it will also bring about poor sodium storage kinetics. The increase in open pore diameter is beneficial for enhancing the slope capacity, thereby improving the sodium storage kinetics. The structure-performance relationships hold promise for guiding the design of HC materials (Fig. 4(f)).

### 2.4. Sodium plating signal of HC

The accurate calibration of the sodium storage capacity of HC materials serves as a fundamental basis for the rational design optimization of SIBs. Furthermore, the identification of non-destructive early-detection indicators for metallic sodium deposition offers critical protection mechanisms to ensure prolonged cycling stability and improved safety performance in SIBs systems. Notably, the aforementioned transition in electrochemical behavior during sodium storage and plating processes can serve as one such reliable early-warning signal for sodium plating occurrence. At the Na||HC half-cell level, there is a clear plateau of sodium plating and sodium stripping in the over-discharge and charge curves compared to normal discharge and charge curves (Fig. 5(a, b)). Incremental capacity (IC) analysis, as a non-destructive electrochemical characterization technique, was employed to investigate the charge storage mechanisms in Na||HC half-cells. IC profile revealed a distinct sodium stripping peak at potentials cathodic to the sodium extraction plateau (Fig. 5(c)), which was further corroborated by GITT measurements. During the sodiation process, the diffusion coefficient of $Na^+$ first decreased, then increased in the plateau region, and rapidly decreased when the potential was below 0 V (Fig. 5(d)). Two voltage plateaus can also be clearly observed in the plateau region of the sodiation profiles (Fig. S26). In the initial stage of the desodiation process, the diffusion coefficient of $Na^+$ increases from an extremely low value (Fig. 5(e)). It can be attributed to the preferential occurrence of metallic sodium stripping over sodium ion extraction during the initial electrochemical process. As demonstrated in Fig. 5(f), the stripping reaction initiates at lower potentials, preceding the subsequent extraction reaction. At the full cell level, a 5 Ah NFPP||HC pouch cell is charged and discharged in environments at 25 °C, 0 °C, and −10 °C, and the discharge curves are differentiated. A noticeable sodium stripping voltage plateau and IC peak appear in the charge process at −10 °C (Fig. 5(g, h)). Therefore, the IC peak characteristics of sodium deposition behavior can effectively

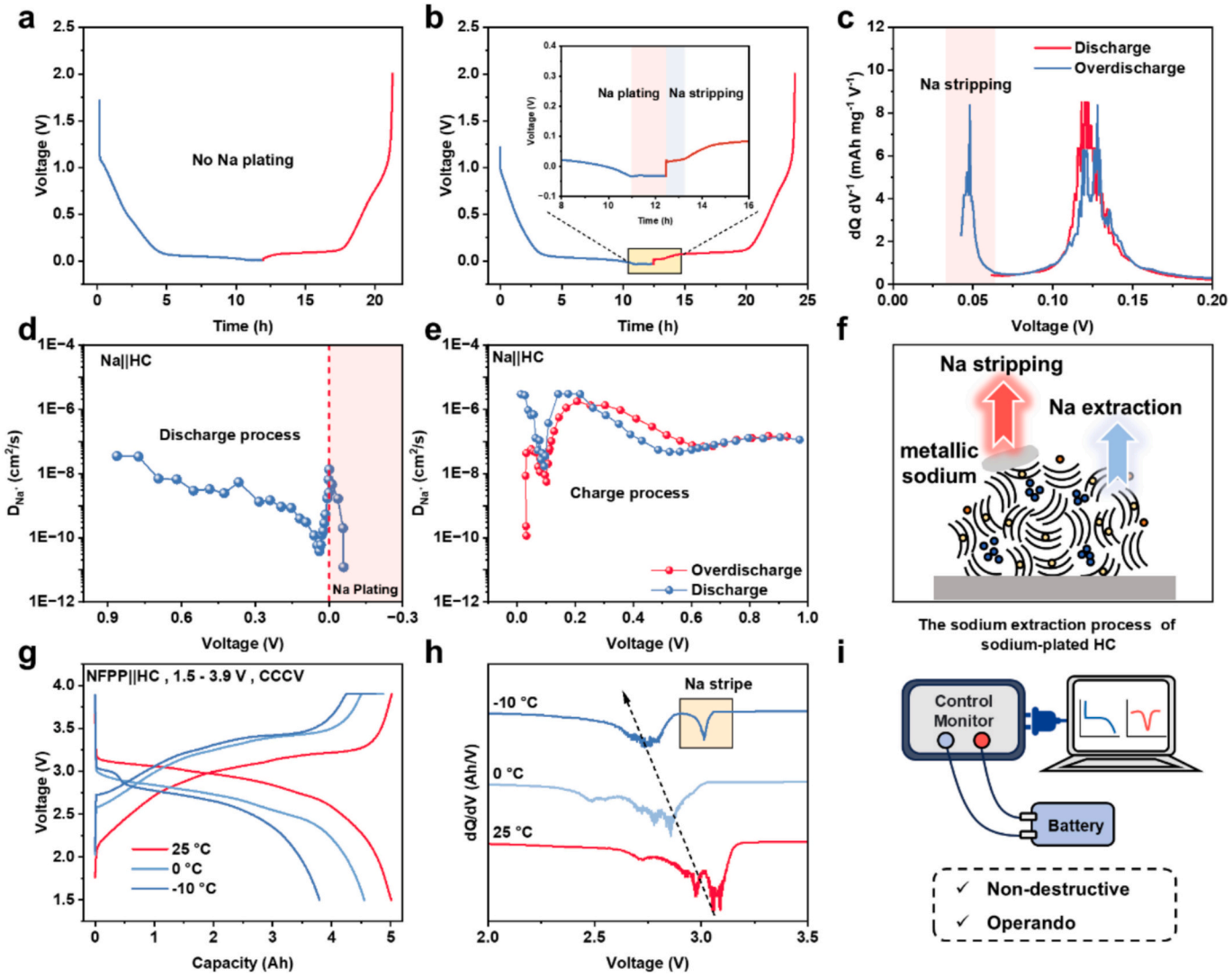


**Fig. 5.** (a) Voltage time profile of Na||HC half-cell during discharge and charging processes. (b) Voltage platform of Na||HC half-cell during over-discharge and charging processes (insert is an enlarged image of the sodium plating platform and sodium stripping platform). (c) IC profiles of charging following over-discharging and discharging. (d) The calculated Na + diffusion coefficients for over-discharge process. (e) The calculated Na + diffusion coefficients for charge process after discharge and over-discharge. (f) Schematic diagram of the process of sodium stripping and the desodiation process of sodiated HC. (g) Discharge/charge profiles of NFPP||HC pouch cell at different temperature. (h) IC profiles of discharging following charging at different temperature. (i) Schematic diagram of the non-destructive extraction of characteristic signals of sodium plating.

serve as a non-destructive early-warning signal to prevent metallic sodium plating, thereby contributing to prolonged cycle life and enhanced safety of SIBs (Fig. 5(i)).

## 3. Conclusion

In this study, the sodium storage mechanism of HC materials was validated through various in-situ characterization methods. In addition, the serious shortcomings of Na||HC half-cells in evaluating HC capacity were fully demonstrated through full cells, and three-electrode cells. Therefore, we propose an innovative capacity determination strategy based on identifying the transition between sodium storage and plating behaviors through electrochemical signatures. Various HC materials were analyzed through in-situ XRD and post-mortem analysis, comprehensively verifying the accuracy and universality of this strategy. Simultaneously, through a statistical comparison of the structural and kinetic characteristics of different HC materials, structural design criteria for improving sodium storage kinetics were revealed, effectively enhancing the rate performance of HC and mitigating risk of metallic sodium plating. Finally, based on this transition of electrochemical behavior, a warning signal for sodium plating behavior was proposed to indicate changes in the safety of SIBs. In summary, this study systematically investigated the sodium storage mechanism, boundaries, kinetics, and sodium plating warning of HC materials, which are expected to have guiding significance for the development and application of long-lifespan and high-safety SIBs.

## CRediT authorship contribution statement

**Wei Li:** Writing – original draft, Investigation, Formal analysis, Data curation, Conceptualization. **Shini Lin:** Formal analysis, Data curation, Conceptualization. **Yuejing Zeng:** Writing – review & editing. **Yuan Qin:** Data curation. **Honghao Xie:** Data curation. **Xing Chen:** Data curation. **Jing Zeng:** Writing – review & editing, Funding acquisition. **Peng Zhang:** Writing – review & editing, Funding acquisition, Formal analysis, Conceptualization. **Jinbao Zhao:** Writing – review & editing, Funding acquisition, Conceptualization.

## Declaration of competing interest

The authors declare that they have no known competing financial interests or personal relationships that could have appeared to influence the work reported in this paper.

## Acknowledgments

We gratefully acknowledge the financial supported by National Key Research and Development Program of China (2021YFB2400300). Natural Science Foundation of Xiamen, China (No. 3502Z202471026). National Natural Science Foundation of China (21875195).

## Appendix A. Supplementary data

Supplementary data to this article can be found online at https://doi.org/10.1016/j.cej.2026.173109.

## Data availability

The data are available on request from the corresponding author.

## References

[1] X. Feng, D. Ren, X. He, M. Ouyang, Mitigating thermal runaway of lithium-ion batteries, Joule 4 (2020) 743–770, https://doi.org/10.1016/j.joule.2020.02.010.
[2] J.B. Goodenough, Y. Kim, Challenges for rechargeable Li batteries, Chem. Mater. 22 (2010) 587–603, https://doi.org/10.1021/cm901452z.
[3] M.A. Hannan, M.M. Hoque, A. Mohamed, A. Ayob, Review of energy storage systems for electric vehicle applications: issues and challenges, Renew. Sust. Energ. Rev. 69 (2017) 771–789, https://doi.org/10.1016/j.rser.2016.11.171.
[4] Q. Wei, T. Huang, X. Huang, B. Wang, Y. Jiang, D. Tang, D.-L. Peng, B. Dunn, L. Mai, High-rate sodium-ion storage of vanadium nitride via surface-redox pseudocapacitance, Interdiscip. Mater. 2 (2023) 434–442, https://doi.org/10.1002/idm2.12080.
[5] H. Song, Y. Li, X.L. Li, Y. Li, D. Li, D. Wang, S. Huang, H.Y. Yang, Recent progress in heterostructured materials for room-temperature sodium-sulfur batteries, Interdiscip. Mater. 3 (2024) 565–594, https://doi.org/10.1002/idm2.12177.
[6] Y.-J. Guo, R.-X. Jin, M. Fan, W.-P. Wang, S. Xin, L.-J. Wan, Y.-G. Guo, Sodium layered oxide cathodes: properties, practicality and prospects, Chem. Soc. Rev. 53 (2024) 7828–7874, https://doi.org/10.1039/D4CS00415A.
[7] E.S. Zsoldos, D.T. Thompson, W. Black, S.M. Azam, J.R. Dahn, The operation window of lithium iron phosphate/graphite cells affects their lifetime, J. Electrochem. Soc. 171 (2024) 080527, https://doi.org/10.1149/1945-7111/ad6cbd.
[8] S. Gao, Z. Zhu, H. Fang, K. Feng, J. Zhong, M. Hou, Y. Guo, F. Li, W. Zhang, Z. Ma, F. Li, Regulation of coordination chemistry for ultrastable layered oxide cathode materials of sodium-ion batteries, Adv. Mater. 36 (2024) 2311523, https://doi.org/10.1002/adma.202311523.
[9] J. Li, H. Hua, X. Deng, P. Lai, Y. Kang, S. Kuang, F. Wang, X. Zeng, Y. Zhang, J. Zhao, Mild and controllable solid electrolyte interphase formation for high-voltage lithium metal batteries in a wide-temperature range from −40°C to 80°C, Chem. Eng. J. 452 (2023) 139398, https://doi.org/10.1016/j.cej.2022.139398.
[10] D. Hubble, D.E. Brown, Y. Zhao, C. Fang, J. Lau, B.D. McCloskey, G. Liu, Liquid electrolyte development for low-temperature lithium-ion batteries, Energy Environ. Sci. 15 (2022) 550–578, https://doi.org/10.1039/D1EE01789F.
[11] F. Ding, C. Zhao, D. Zhou, Q. Meng, D. Xiao, Q. Zhang, Y. Niu, Y. Li, X. Rong, Y. Lu, L. Chen, Y.-S. Hu, A novel Ni-rich O3-Na[Ni0.60Fe0.25Mn0.15]O2 cathode for Na-ion batteries, Energy Storage Mater. 30 (2020) 420–430, https://doi.org/10.1016/j.ensm.2020.05.013.
[12] Y. Liu, X. Wu, A. Moeez, Z. Peng, Y. Xia, D. Zhao, J. Liu, W. Li, Na-rich Na3V2(PO4)3 cathodes for long cycling rechargeable sodium full cells, Adv. Energy Mater. 13 (2023) 2203283, https://doi.org/10.1002/aenm.202203283.
[13] W. Li, H. Xie, S. Lin, Y. Qin, J. Zeng, P. Zhang, J. Zhao, Insights on the degradation mechanism of 7 Ah sodium ion batteries at different aging modes, J. Power Sources 639 (2025) 236635, https://doi.org/10.1016/j.jpowsour.2025.236635.
[14] W. Zheng, G. Liang, Q. Liu, J. Li, J.A. Yuwono, S. Zhang, V.K. Peterson, Z. Guo, The promise of high-entropy materials for high-performance rechargeable Li-ion and Na-ion batteries, Joule 7 (2023) 2732–2748, https://doi.org/10.1016/j.joule.2023.10.016.
[15] J. Hu, X. Li, Q. Liang, L. Xu, C. Ding, Y. Liu, Y. Gao, Optimization strategies of Na3V2(PO4)3 cathode materials for sodium-ion batteries, Nano-Micro Lett. 17 (2024) 33, https://doi.org/10.1007/s40820-024-01526-x.
[16] H. Li, W. Ji, P. Zhang, J. Zhao, Safety boundary of power battery based on quantitative lithium deposition, J. Energy Storage 52 (2022) 104789, https://doi.org/10.1016/j.est.2022.104789.
[17] X. Wang, Q. Zhang, C. Zhao, H. Li, B. Zhang, G. Zeng, Y. Tang, Z. Huang, I. Hwang, H. Zhang, S. Zhou, Y. Qiu, Y. Xiao, J. Cabana, C.-J. Sun, K. Amine, Y. Sun, Q. Wang, G.-L. Xu, L. Gu, Y. Qiao, S.-G. Sun, Achieving a high-performance sodium-ion pouch cell by regulating intergrowth structures in a layered oxide cathode with anionic redox, Nat. Energy 9 (2024) 184–196, https://doi.org/10.1038/s41560-023-01425-2.
[18] C. Zhao, Q. Wang, Z. Yao, J. Wang, B. Sánchez-Lengeling, F. Ding, X. Qi, Y. Lu, X. Bai, B. Li, H. Li, A. Aspuru-Guzik, X. Huang, C. Delmas, M. Wagemaker, L. Chen, Y.-S. Hu, Rational design of layered oxide materials for sodium-ion batteries, Science 370 (2020) 708–711, https://doi.org/10.1126/science.aay9972.
[19] B. Zhang, G. Chen, Y. Yang, M. Liu, X. Li, H. Liu, Z.-F. Ma, Heterovalent chromium-doped Na3Fe2(PO4)P2O7 cathode material with superior rate and stability performance for sodium-ion storage, ACS Sustain. Chem. Eng. 11 (2023) 10083–10094, https://doi.org/10.1021/acssuschemeng.3c02013.
[20] X. Pu, H. Wang, T. Yuan, S. Cao, S. Liu, L. Xu, H. Yang, X. Ai, Z. Chen, Y. Cao, Na4Fe3(PO4)2P2O7/C nanospheres as low-cost, high-performance cathode material for sodium-ion batteries, Energy Storage Mater. 22 (2019) 330–336, https://doi.org/10.1016/j.ensm.2019.02.017.
[21] L. Li, Z. Hu, Y. Lu, C. Wang, Q. Zhang, S. Zhao, J. Peng, K. Zhang, S.-L. Chou, J. Chen, A low-strain potassium-rich Prussian blue analogue cathode for high power potassium-ion batteries, Angew. Chem. Int. Ed. 60 (2021) 13050–13056, https://doi.org/10.1002/anie.202103475.
[22] H. Yang, Q. Zhang, M. Chen, Y. Yang, J. Zhao, Unveiling the origin of air stability in Polyanion and layered-oxide cathode materials for sodium-ion batteries and their practical application considerations, Adv. Funct. Mater. 34 (2024) 2308257, https://doi.org/10.1002/adfm.202308257.
[23] J.C. Hyun, H.M. Jin, J.H. Kwak, S. Ha, D.H. Kang, H.S. Kim, S. Kim, M. Park, C. Y. Kim, J. Yoon, J.S. Park, J.-Y. Kim, H.-D. Lim, S.Y. Cho, H.-J. Jin, Y.S. Yun, Design guidelines for a high-performance hard carbon anode in sodium ion batteries, Energy Environ. Sci. 17 (2024) 2856–2863, https://doi.org/10.1039/D4EE00315B.
[24] D. Chen, W. Zhang, K. Luo, Y. Song, Y. Zhong, Y. Liu, G. Wang, B. Zhong, Z. Wu, X. Guo, Hard carbon for sodium storage: mechanism and optimization strategies toward commercialization, Energy Environ. Sci. 14 (2021) 2244–2262, https://doi.org/10.1039/D0EE03916K.
[25] Z. Cheng, H. Zhang, J. Cui, J. Zhao, S. Dai, Z. Zhang, K. Song, S. Wang, Y. Yuan, Q. Chen, X. Kong, L. Qie, L. Yuan, H. Yang, S. Zhu, Y. Fang, Y. Huang, Y. Yao, Interlayer-expanded carbon anodes with exceptional rates and long-term cycling via kinetically decoupled carbonization, Joule 9 (2025) 101812, https://doi.org/10.1016/j.joule.2024.101812.
[26] Q. Meng, Y. Lu, F. Ding, Q. Zhang, L. Chen, Y.-S. Hu, Tuning the closed pore structure of hard carbons with the highest Na storage capacity, ACS Energy Lett. 4 (2019) 2608–2612, https://doi.org/10.1021/acsenergylett.9b01900.
[27] J. Liu, Y. You, L. Huang, Q. Zheng, Z. Sun, K. Fang, L. Sha, M. Liu, X. Zhan, J. Zhao, Y.-C. Han, Q. Zhang, Y. Chen, S. Wu, L. Zhang, Precisely tunable instantaneous carbon rearrangement enables low-working-potential hard carbon toward sodium-ion batteries with enhanced energy density, Adv. Mater. 36 (2024) 2407369, https://doi.org/10.1002/adma.202407369.
[28] Y. Zeng, F. Wang, Y. Cheng, M. Chen, J. Hou, D. Yang, Y. Zhang, W. Yang, G. Liu, Y. Zhang, Z. Zhu, X. Li, Y. Yang, J. Zhao, Identifying the importance of functionalization evolution during pre-oxidation treatment in producing economical asphalt-derived hard carbon for Na-ion batteries, Energy Storage Mater. 73 (2024) 103808, https://doi.org/10.1016/j.ensm.2024.103808.
[29] X. Wang, J. Lu, Y. Wu, W. Zheng, H. Zhang, T. Bai, H. Liu, D. Li, L. Ci, Building stable anodes for high-rate Na-metal batteries, Adv. Mater. 36 (2024) 2311256, https://doi.org/10.1002/adma.202311256.
[30] J. Patra, H.-T. Huang, W. Xue, C. Wang, A.S. Helal, J. Li, J.-K. Chang, Moderately concentrated electrolyte improves solid–electrolyte interphase and sodium storage performance of hard carbon, Energy Storage Mater. 16 (2019) 146–154, https://doi.org/10.1016/j.ensm.2018.04.022.
[31] R. Dong, L. Zheng, Y. Bai, Q. Ni, Y. Li, F. Wu, H. Ren, C. Wu, Elucidating the mechanism of fast Na storage kinetics in ether electrolytes for hard carbon anodes, Adv. Mater. 33 (2021) 2008810, https://doi.org/10.1002/adma.202008810.
[32] C. Qiu, A. Li, D. Qiu, Y. Wu, Z. Jiang, J. Zhang, J. Xiao, R. Yuan, Z. Jiang, X. Liu, X. Chen, H. Song, One-step construction of closed pores enabling high plateau capacity hard carbon anodes for sodium-ion batteries: closed-pore formation and energy storage mechanisms, ACS Nano 18 (2024) 11941–11954, https://doi.org/10.1021/acsnano.4c02046.
[33] G. Liu, Z. Wang, H. Yuan, C. Yan, R. Hao, F. Zhang, W. Luo, H. Wang, Y. Cao, S. Gu, C. Zeng, Y. Li, Z. Wang, N. Qin, G. Luo, Z. Lu, Deciphering electrolyte dominated Na+ storage mechanisms in hard carbon anodes for sodium-ion batteries, Adv. Sci. 10 (2023) 2305414, https://doi.org/10.1002/advs.202305414.
[34] M. Liu, Z. Jiang, X. Wu, F. Liu, W. Li, D. Meng, A. Wei, P. Nie, W. Zhang, W. Zheng, Reinventing the high-rate energy storage of hard carbon: the order-degree governs the trade-off of desolvation-solid electrolyte interphase at interfaces, Angewandte Chemie International Edition n/a (n.d.) e202425507. doi:https://doi.org/10.1002/anie.202425507.
[35] W. Li, S. Lin, H. Xie, Y. Qin, Q. Wu, J. Zeng, P. Zhang, J. Zhao, Uncovering Sodiated HC dominated thermal runaway mechanism of NFPP/HC pouch battery, Appl. Energy 391 (2025) 125936, https://doi.org/10.1016/j.apenergy.2025.125936.
[36] Y. Zeng, J. Yang, H. Yang, Y. Yang, J. Zhao, Bridging microstructure and sodium-ion storage mechanism in hard carbon for sodium ion batteries, ACS Energy Lett. 9 (2024) 1184–1191, https://doi.org/10.1021/acsenergylett.3c02751.
[37] X.-X. He, W.-H. Lai, Y. Liang, J.-H. Zhao, Z. Yang, J. Peng, X.-H. Liu, Y.-X. Wang, Y. Qiao, L. Li, X. Wu, S.-L. Chou, Achieving all-plateau and high-capacity sodium insertion in topological graphitized carbon, Adv. Mater. 35 (2023) 2302613, https://doi.org/10.1002/adma.202302613.
[38] X. Chen, J. Tian, P. Li, Y. Fang, Y. Fang, X. Liang, J. Feng, J. Dong, X. Ai, H. Yang, Y. Cao, An overall understanding of sodium storage behaviors in hard carbons by

an “adsorption-intercalation/filling” hybrid mechanism, Adv. Energy Mater. 12 (2022) 2200886, https://doi.org/10.1002/aenm.202200886.
[39] L.J. Hardwick, P.W. Ruch, M. Hahn, W. Scheifele, R. Kötz, P. Novák, *In situ* Raman spectroscopy of insertion electrodes for lithium-ion batteries and supercapacitors: first cycle effects, J. Phys. Chem. Solids 69 (2008) 1232–1237, https://doi.org/10.1016/j.jpcs.2007.10.017.
[40] N. Sun, J. Qiu, B. Xu, Understanding of sodium storage mechanism in hard carbons: ongoing development under debate, Adv. Energy Mater. 12 (2022) 2200715, https://doi.org/10.1002/aenm.202200715.
[41] Z. Tang, R. Zhang, H. Wang, S. Zhou, Z. Pan, Y. Huang, D. Sun, Y. Tang, X. Ji, K. Amine, M. Shao, Revealing the closed pore formation of waste wood-derived hard carbon for advanced sodium-ion battery, Nat. Commun. 14 (2023) 6024, https://doi.org/10.1038/s41467-023-39637-5.
[42] K.-Y. Zhang, H.-H. Liu, J.-M. Cao, J.-L. Yang, M.-Y. Su, X.-Y. Wang, Z.-Y. Gu, J. Wang, B. Li, Y. Wang, X.-L. Wu, Microstructure reconstruction via confined carbonization achieves highly available sodium ion diffusion channels in hard carbon, Energy Storage Mater. 73 (2024) 103839, https://doi.org/10.1016/j.ensm.2024.103839.
[43] L. Wang, Z. Xu, P. Lin, Y. Zhong, X. Wang, Y. Yuan, J. Tu, Oxygen-crosslinker effect on the electrochemical characteristics of asphalt-based hard carbon anodes for sodium-ion batteries, Advanced Energy Materials n/a (n.d.) 2403084. doi:https://doi.org/10.1002/aenm.202403084.
[44] S. Manna, P. Verma, S. Puravankara, Correlating storage mechanism and solid electrolyte interphase kinetics for high-rate performance of hard carbon anode in ether electrolytes for sodium-ion batteries, J. Power Sources 631 (2025) 236234, https://doi.org/10.1016/j.jpowsour.2025.236234.
[45] G. Liu, Z. Wang, H. Yuan, C. Yan, R. Hao, F. Zhang, W. Luo, H. Wang, Y. Cao, S. Gu, C. Zeng, Y. Li, Z. Wang, N. Qin, G. Luo, Z. Lu, Deciphering electrolyte dominated Na+ storage mechanisms in hard carbon anodes for sodium-ion batteries, Adv. Sci. 10 (2023) 2305414, https://doi.org/10.1002/advs.202305414.
[46] X. Yin, Z. Wang, Y. Liu, Z. Lu, H. Long, T. Liu, J. Zhang, Y. Zhao, Insight into the influence of ether and ester electrolytes on the sodium-ion transportation kinetics for hard carbon, Nano Res. 16 (2023) 10922–10930, https://doi.org/10.1007/s12274-023-5793-9.
[47] L. Yan, G. Zhang, J. Wang, Q. Ren, L. Fan, B. Liu, Y. Wang, W. Lei, D. Ruan, Q. Zhang, Z. Shi, Revisiting electrolyte kinetics differences in sodium ion battery: are esters really inferior to ethers? Energy Environ. Mater. 6 (2023) e12523 https://doi.org/10.1002/eem2.12523.
[48] B.B. Frey, The SAGE Encyclopedia of Educational Research, Measurement, and Evaluation, SAGE Publications, Inc., 2018, https://doi.org/10.4135/9781506326139.
[49] G. Huang, H. Zhang, F. Gao, D. Zhang, Z. Zhang, Y. Liu, Z. Shang, C. Gao, L. Luo, M. Terrones, Y. Wang, Overview of hard carbon anode for sodium-ion batteries: influencing factors and strategies to extend slope and plateau regions, Carbon 228 (2024) 119354, https://doi.org/10.1016/j.carbon.2024.119354.
[50] L. Guo, M. Huang, W. Liu, H. Zhu, Y. Cheng, M.-S. Wang, Pore-size tuning of hard carbon to optimize its wettability for efficient Na+ storage, J. Mater. Chem. A 12 (2024) 13703–13712, https://doi.org/10.1039/D4TA02303J.